Tribol Lett (2016)62:26
DOI 10.1007/s11249-016-0673-z

ORIGINAL PAPER

Investigating the Process of White Etching Crack Initiation in Bearing Steel

Benjamin Gould[1,2] · **Aaron Greco**[1]

Received: 27 January 2016 / Accepted: 14 March 2016

Abstract White etching cracks (WECs) have been identified as a dominant mode of premature failure within wind turbine gearbox bearings. Though WECs have been reported in the field for over a decade, the conditions leading to WECs and the process by which this failure culminates are both highly debated. In previously published work, the generation of WECs on a benchtop scale was linked to sliding at the surface of the test sample, and it was also postulated that the generation of WECs was dependent on the cumulative energy that had been applied to the sample over the entirety of the test. In this paper, a three-ring-on-roller benchtop test rig is used to systematically alter the cumulative energy that a sample experiences through changes in normal load, sliding, and run-time, in an attempt to correlate cumulative energy with the formation of WECs. It was determined that, in the current test setup, the presence of WECs can be predicted by this energy criterion. The authors then used this information to study the process by which WECs initiate. It was found that, under the current testing conditions, the formation of a dark etching microstructure precedes the formation of a crack, and a crack precedes the formation of white etching microstructure.

Keywords White etching cracks · Wind turbine gearbox bearings · Microstructural alterations · Bearing failures

✉ Benjamin Gould
Bengould@udel.edu

[1] Energy Systems Division, Argonne National Laboratory, Lemont, IL, USA

[2] Department of Mechanical Engineering, University of Delaware, Newark, DE, USA

1 Introduction

Wind turbine gearboxes often exhibit unpredictable and premature failures [1, 2]; these failures are the leading cause of downtime in wind turbines and incur significant maintenance costs on wind plant operators and original equipment manufacturers [3, 4]. The majority of gearbox failures initiate at bearings, and the dominant failure mode in these bearings is axial cracking associated with local microstructural alterations [4]. The formation of these cracks can lead to failures in as little as 5–10 % of the bearing's design life [as defined by L_{10} based on classical rolling contact fatigue (RCF)] [5–7]. Typically, these failures have been referred to as white etching cracks (WECs), due the fact that the resulting altered microstructure, referred to as white etching area (WEA), appears white when etched with Nital. Additional terminology used to describe this failure mode includes white structure flaking, irregular white structure flaking, and brittle flaking [8]. Recent work has stated that the most progressed stage of the microstructural alterations that are associated with these cracks is that of nano-grain ferrite surrounded by carbon at its grain boundaries [9]. It has also been observed that other forms of microstructural alterations, which appear dark when etched with Nital, likely precede the formation of this white etching nano-grain ferrite [10–12]. WECs are traditionally characterized by the existence of WEA; however, it is currently unknown wheather the WEA contributes to the failure process in any way, or whether it simply a symptom of a previously initiated failure, e.g., a crack.

Within steel bearings, white etching alterations of any kind fundamentally form due to large local energies which aid in atomic diffusion or recrystallization. Examples of this have been previously observed in classical rolling

Published online: 01 April 2016

contact fatigue (RCF), scuffing, and micro-pitting. In classical RCF, it has been reported that bearings which were operating at high temperature, or under high contact pressure, would exhibit dark etching areas (DEA) localized at a depth corresponding to the area of maximum shear stress based on the contact pressure, followed by the formation of white etching bands (WEBs) [13–16]. In scuffing, sliding surfaces experience an instantaneous high frictional energy event that leads to a catastrophic failure and the formation of a white etching microstructure on the scuffed surface [17, 18]. This alteration is thought to be the result of an instability condition in which the frictional heat input localized at the contact surface exceeds a critical material limit [17]. In micro-pitting, white etching alterations form near surface under pits resulting from asperity contact, and it is postulated that the high localized shear and normal stresses associated with contact at the asperities leads to the formation of these alterations [19]. The specific conditions that lead to each one of these failures are distinctly different; however, the formation of the white etching alterations that are associated with each of these failure modes can be linked to the exceeding of an energy threshold (instantaneous or cumulative) that allows for the alteration to form.

Within wind turbines, the conditions that lead to the formation of the alterations associated with WECs are highly debated and ultimately unknown. However, these alterations could be due to any driver that leads to energy being input into the system, and this includes but is not limited to: applied strain due to normal loading or impact loading associated with torque reversals [20], thermal heat from high friction or sliding that occurs during transient acceleration and decelerations [21], or electrical discharge from stray currents stemming from the generator or other components [8]. Additionally, the steel structure could be compromised through embrittlement by externalities such as atomic hydrogen. The sources of hydrogen or other embrittling factors could be due to lubricant decomposition [22], or water contamination [23–25]. In theory, embrittlement of any source would reduce the energy threshold required to form a microstructural alteration. However, energy inputs, such as those discussed above, would still be required in order to drive this process.

Accelerated benchtop tests capable of reproducing WECs are necessary to study both the drivers that lead to their formation, as well as methods that can be used to prevent them. Numerous studies have recreated WECs by charging test samples with hydrogen [13, 23–37], which, as stated above, eases the formation of microstructural alterations. However, embrittling samples before testing imposes a condition that is not necessarily known to occur in wind turbine gearboxes; therefore, recent work has shifted toward WEC reproduction in non-charged samples. WECs have been reproduced at a benchtop scale without charging in three different types of test bearings: deep-groove ball bearings [36, 38], cylindrical roller thrust bearings [38, 39], and spherical roller bearings [40]. The limitation with studying the formation of WECs within test bearings is that the experimental conditions are constrained by the bearing geometry and testing rig. For example, the amount of slip that each one of the previously listed bearing contacts sees is a geometric constraint and cannot be altered; therefore, slip cannot be studied as an independent WEC driver. Additionally, it is often difficult to study drivers such as lubrication condition or loading, due to oil and test rig constraints, respectively.

Recently, WECs have been replicated through the use of a three-ring-on-roller benchtop test rig [10]. This marked the first time that this failure mode had been reproduced without hydrogen charging, in a testing rig that allows for a high degree of controllability of operational conditions, specifically slide-to-roll percentage. While the exact level of sliding (or any other contact condition) experienced in a wind turbine bearing is largely unknown, it is thought that sliding does occur as a result of load zone reversals on the bearing or changes in rotation speed. Therefore, a study of influence that sliding and lubrication conditions have on the formation of WECs was performed. It was found that an increase in the sliding magnitude as well as changing the sliding direction (positive vs negative sliding) aided in the formation of WECs. High sliding (15 % slip) in the negative direction (the surface traction force opposed the direction of surface motion) was the only condition of those studied that leads to WEC generation. It was also suggested that the formation of the microstructural alterations associated with these cracks is dependent on the cumulative energy applied to the sample over the runtime of the test. The aim of the current work is to investigate the initiation process of WECs and to determine whether a correlation exists between the point of WEC initiation and the cumulative energy applied to a sample within a rolling sliding contact. For this study, the applied energy will be controlled through variations in test parameters including load, sliding ratio, and test duration.

2 Materials/Testing

All tests were performed on a PCS Instruments micro-pitting rig (MPR), shown in Fig. 1. The MPR provides a three-ring-on-roller splash lubricated line contact and allows for testing at customizable user-specified conditions. The MPR can be operated at slide-to-roll ratios ranging from pure rolling to pure sliding, at loads ranging from 0.5 to 3 GPa, and at lubricant temperatures in excess of 100 °C. In addition to this, the authors have incorporated a Julabo 1201 convective cooler with a customized control

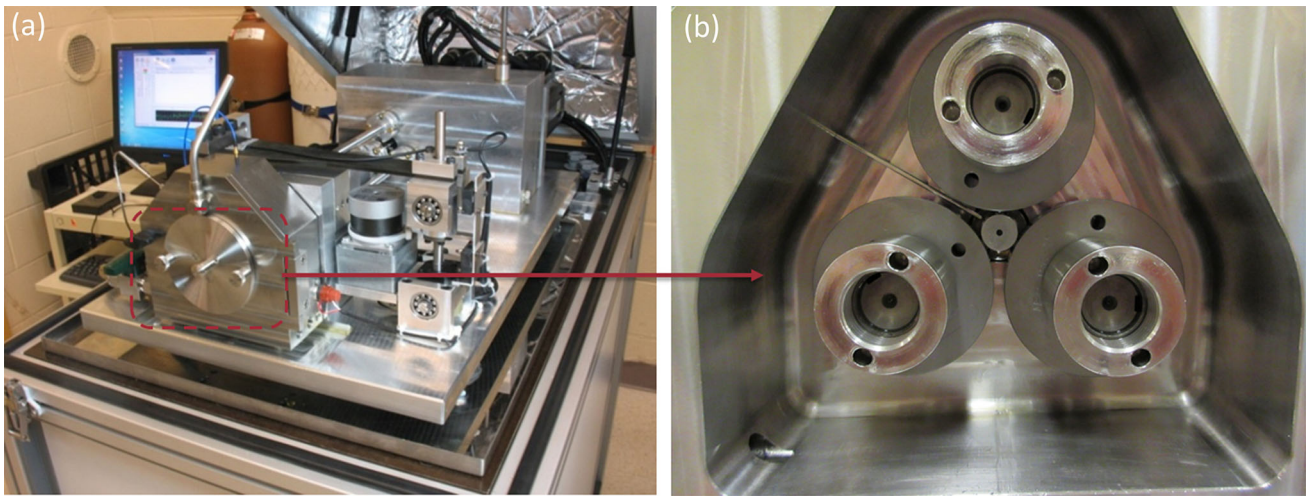

Fig. 1 PCS Instruments micro-pitting rig (MPR), which contains (**a**) *three-ring*-on-roller contact, shown in **b**, used to simulate rolling/sliding between a bearing roller and raceway. Permission obtained from Springer and published in Tribology Letters via license number 3835481289370 [10]

loop, which is used to maintain prescribed oil temperatures when the contact conditions generate a large amount of frictional heat, such as tests that require both high sliding and high load.

The test specimen that is examined for WECs throughout this paper is the 12-mm-diameter central roller, shown in Fig. 2. This roller has a 1-mm-wide initial wear track that comes in contact with each of the three 54-mm-diameter rings. All of the experiments presented use AISI 52100 through hardened tempered martensitic steel for both the rollers and rings. The supplier-provided specific composition of this steel is shown in Table 1. The Rockwell C hardness of the rollers and the rings was measured as 60 and 63, respectively.

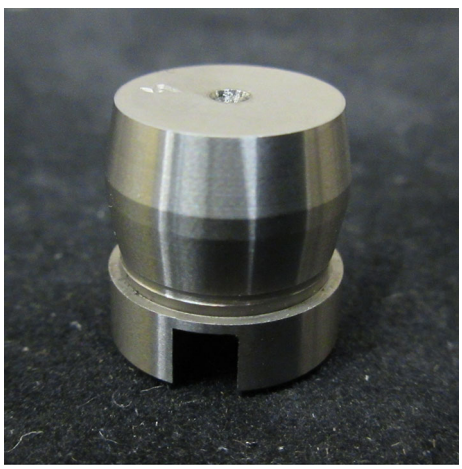

Fig. 2 12-mm-diameter test roller used in the MPR, and it is placed in the center of the three rings as shown in Fig. 1b. Permission obtained from Springer and published in Tribology Letters via license number 3835481289370 [10]

The lubricant used in this study is a group IV synthetic, viscosity grade 68, fully formulated gear oil. The metallic content of the oil was determined though inductively coupled plasma mass spectrometry (ICP-MS), all detected metals that returned quantities of >1 ppm are shown in Table 2. This lubricant is similar to that which has been used in previous WEC studies [10, 39].

An accelerometer was used to monitor the vibration resulting from the roller/ring contact during the tests. Tests were concluded when either a vibration level corresponding to the formation of significant surface damage was detected or the roller had experienced 100 million contact cycles. After each test finished, the respective rollers were sectioned circumferentially through the wear track, as shown in Fig. 3, mounted in Bakelite, and polished to multiple locations along the wear track using a sequence of 220 grit grinding followed by 9-, 3-, and 1-μm diamond polishing medium. At each section, the samples were etched with a 3 % Nital solution in order to examine the subsurface for microstructural alterations. Additional analysis was performed on a FEI Quanta 400F environmental scanning electron microscope (SEM). The number of sectioning steps performed was determined through the observation of WECs; rollers which contained no observable WECs were polished to a minimum of five locations at least 100 μm apart, while rollers that contained a noticeable number of WECs were examined at a fewer number of sections.

As stated earlier, the microstructural alterations that are observed in wind turbine gearbox bearings must form due to large local energy that promotes atomic diffusion or recrystallization. Within wind turbines, this energy could include but not be limited to: strain energy due to the Hertzian stresses of over-rolling, energy due to impact

Table 1 Chemical composition (provided by supplier) of the AISI 52100 martensitic through hardened steel used in the MPR tests, and all values are given in percentage weight

C	Si	Mn	P	S	Cr	Mo	Ni	Cu	Sn	Al	V	Ca
.9600	.2600	.4200	.0250	.0030	1.4700	.0340	.1200	.2000	.0170	.0100	.0060	.0001

Table 2 Metallic content of the gear oil used in all tests presented, as detected by ICP-MS

Metal detected	Quantity detected
Sodium (Na)	>1000 ppm
Boron (B)	720 ppm
Zinc (Zn)	1970 ppm
Phosphorus (P)	1698 ppm
Calcium (Ca)	3811 ppm
Magnesium (Mg)	8 ppm
Potassium (K)	3 ppm

loads associated with torque reversals [20], thermal heat energy generated during transient events that lead to sliding [21], and electrical discharge due to improper grounding [1]. While all of these energy inputs could have an effect on the generation of WECs, the aim of the current paper is to attempt to find a correlation between the cumulative frictional heat energy applied to a roller over the lifetime of the test, and the presence of WECs in test rollers. If a correlation is found, then it should be possible to predict the formation of WECs, in the current experimental setup, based on the cumulative applied frictional heat energy. This would enable a study of the process by which these failures initiate in bearing steel.

Neglecting any heat loss to the surroundings, accounting for frictional heat generation at the three-ring-on-roller contacts, and assuming half of the energy generated at each contact is input into the ring and half is input into the roller, the cumulative frictional heat energy that the roller experiences over the entirety of the test is shown in Eq. 1. In this equation, ΔV is the sliding speed (the difference between the velocity of the ring and the velocity of the roller at the contact), μ is the average measured friction coefficient, N is the normal load, and t is the total testing time.

$$E = \frac{3}{2}\Delta V \mu N t \tag{1}$$

In order to investigate the hypothesis that, under the current testing conditions, the cumulative energy applied to a sample can be used to predict the formation of WECs, a testing plan was developed that systematically varies the cumulative frictional heat energy that test rollers experience through changes in run-time, normal load, and sliding velocity. It should be reiterated that frictional heat energy

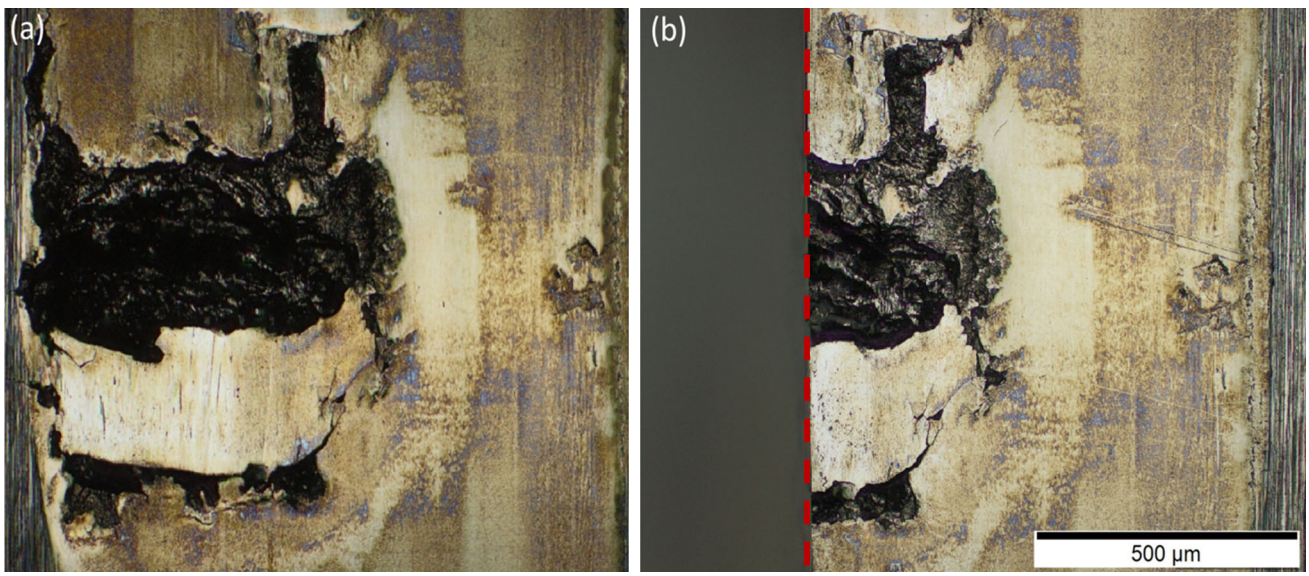

Fig. 3 Optical microscope images of the roller track for Test 1, showing the pitted surface **a** before and **b** after sectioning in the circumferential direction. The *dotted red line* represents the section that was taken in order to investigate whether WECs were present in the subsurface of the roller (Color figure online)

is not the only energy input affecting the rollers during the test; however, we believe that, under these current testing conditions, this frictional heat energy input could be significant enough to correlate with WEC formation. It should also be kept in mind that correlation does not imply causation and that the main use of any correlation found is to study the initiation of WECs. The parameters for all tests conducted in this paper are shown in Table 3. Tests 1–4, which were previously reported in [10], investigate changes in the cumulative frictional heat energy due to changes in the slide-to-roll ratio (SRR) and therefore ΔV in Eq. 1. The formula for calculating the SRR within the MPR can be seen in Eq. 2. Tests 5–8 examine changes in the cumulative frictional heat energy due to normal load (N), and Tests 1, 9, and 10 investigate changes in the cumulative frictional heat energy due to run-time (t). Tests 11 and 12 were both designed to study the onset of WECs based on the runtime results determined in Tests 1–10. The correlation used to determine the parameters of Tests 11–12 will be discussed in detail later.

$$SRR(\%) = \left(\frac{2 \cdot \left(U_{Ring} - U_{Roller}\right)}{U_{Ring} + U_{Roller}}\right) \times 100 \quad (2)$$

A measure of WECs per cross section is used in order to compare the twelve tests in this paper. This term refers to the number of independent WECs that were tallied for a given sample, averaged over the number of cross sections examined for that sample. An example of this measure is as follows: If a roller is sectioned circumferentially and polished to three different axial locations throughout the wear track, and 30, 33, and 35 independent WECs were found, then the value of WECs per cross section would be $(30 + 33 + 35)/3 = 32.67$. It should be noted that it is possible for two WECs which are seemingly independent at one cross section to intersect at a different axial position that was not examined; therefore, the term "independent WECs" does not necessarily mean total WECs. Additionally, the measure of WECs per cross section is used to simply represent the observation of how widespread the WECs are for a given sample. Because the aim of this study is to establish a criterion for initiation of WECs, it should be emphasized that the presence of WECs is much more important than the number of WECs.

3 Results

Of the twelve tests performed, six generated WECs (Tests 1, 6, 7, 8, 10, and 12) and six did not (Tests 2, 3, 4, 5, 9, and 11). The tests that generated WECs also corresponded to the six highest values of cumulative frictional heat energy, and this data are shown in Table 3. Characteristic images of the WECs that were generated in Tests 1, 6, 7, 8, 10, and 12 are shown in Fig. 4.

Figure 5a is a chart that shows the number of WECs generated versus the cumulative frictional heat energy for Tests 1–4. In Tests 1–4, the sliding magnitude and direction were varied through changes in the SRR, and these tests corresponded to SRRs of −30, 30, −5, and 5 %, respectively. It is shown that Test 1, which was run at −30 %SRR, had the largest cumulative applied frictional heat energy and was the only test of these four that generated WECs. This high cumulative frictional heat energy was due to the combination of a high sliding velocity when compared to Tests 3 and 4, and a longer run-time when compared to Test 2.

Table 3 Testing parameters for the 12 tests conducted, as well as the number of contact cycles the roller experienced, whether WECs were found in the roller, and the cumulative frictional heat energy

Test #	Load (N)	Contact stress (GPa)	Rolling speed (m/s)	SRR (%)	Composite roughness Ra (nm)	Temp (°C)	λ	Contact cycles (10^6)	Were WECs found?	Cumulative frictional energy (MJ)
1	500	1.9	1	−30	553	100	.06	38.2	Yes	8.04
2	500	1.9	1	+30	651	100	.06	18.2	No	3.32
3	500	1.9	1	−5	660	100	.06	100	No	3.52
4	500	1.9	1	+5	608	100	.06	34.5	No	1.03
5	40	0.5	3.4	−30	633	100	.18	100	No	2.89
6	135	1.0	3.4	−30	494	100	.20	100	Yes	7.93
7	300	1.5	3.4	−30	488	100	.18	100	Yes	13.14
8	500	1.9	3.4	−30	497	100	.17	42.0	Yes	9.70
9	500	1.9	1	−30	618	100	.05	20	No	4.63
10	500	1.9	1	−30	655	100	.05	30	Yes	6.26
11	500	1.9	2	−15	502	100	.12	21.8	No	2.14
12	300	1.5	3.4	−30	504	100	.17	85	Yes	8.60

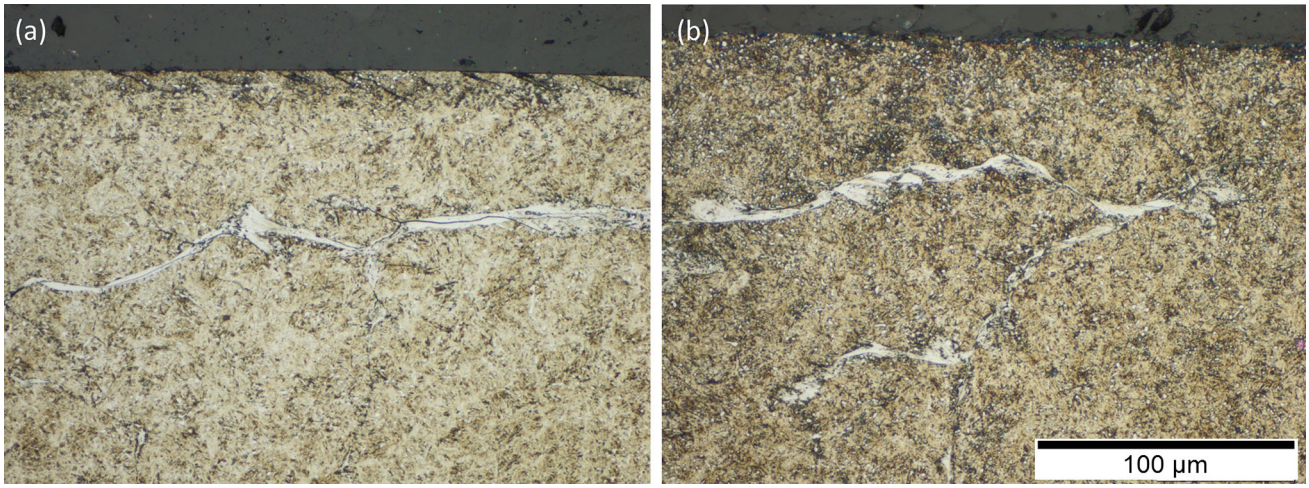

Fig. 4 Optical images of etched circumferential cross sections showing cracks generated in **a** Test 8 and **b** Test 9, and these images are characteristic of the WECs that formed in Tests 1, 6, 7, 8, 10, and 12

Figure 5b corresponds to Tests 5–8 where the contact stress was systematically varied from 0.5 to 1.9 GPa through changes in load. This chart shows that the three tests with the highest cumulative frictional heat energy generated WECs, and these tests corresponded contact stresses of 1.0, 1.5, and 1.9 GPa. It is worth noting that the rate of frictional heat energy application increases linearly with load; however, the cumulative frictional heat energy does not. Test 7 (1.5 GPa) had a larger cumulative frictional heat energy than that of Test 8 (1.9 GPa), even though Test 8 had higher rate of frictional heat energy application. This was due to the fact that the contact conditions of Test 8 led to the formation of a macro-pit at 42.0 million cycles, while Test 7 reached the run out limit of 100 million cycles. This increase in run-time was seemingly caused by a decrease in the rate of crack propagation due to the decreased load; the validity of this statement will be investigated in detail later.

Figure 5c corresponds to Tests 1, 9, and 10, where only the test run-time was varied. After it was observed that Test 1 generated WECs, Tests 9 and 10 were intentionally run under the same contact conditions, but stopped prior to the predicted failure point. Test 1 formed a macro-pit at 38.2 million cycles; therefore, Tests 9 and 10 were stopped at 20 and 30 million cycles, respectively. It was found that Test 9 did not generate WECs; however, Test 10 did. The findings of these tests, pertaining to the process by which WECs initiate, will be discussed in detail later.

Finally, Fig. 5d contains all of the data from the previous three studies corresponding to Tests 1–10. This chart shows that, under these testing conditions, the cumulative frictional heat energy can be used to predict the presence of WECs within a test roller. Specifically, WECs will form when the cumulative frictional heat energy exceeds a threshold of somewhere between 4.6 and 6.3 MJ.

After the correlation between cumulative frictional heat energy and WEC generation was determined, Test 11 was designed in order to study how changing the test conditions, but leaving the rate of energy application the same, leads to different failure modes. Test 12 was designed in order to differentiate between the drivers of WEC initiation and WEC propagation. These tests are not included in the above figures; however, they are discussed in detail below.

4 Discussion

4.1 Initiation Versus Propagation

The formation of a WEC-induced macro-pit can be described in two stages, WEC initiation and WEC propagation. WEC initiation refers to the process by which a crack with associated WEA forms within a sample; in this study, this refers to the time period from the start of a test to the first instance where a crack with adjacent WEA exists. WEC propagation refers to the process by which this pre-existing crack propagates to a macro-pit. It should be acknowledged that these two stages could (and likely do) have independent drivers. These drivers can be examined by comparing Test 7 and Test 12. Test 7 was run at a load corresponding to 1.5 GPa contact pressure; this test had the largest cumulative frictional heat energy of any test in this paper. However, it is argued that the reason for this large cumulative energy was that the WECs that formed in the subsurface of this sample propagated much slower when compared to tests that were ran at 1.9 GPa. Therefore, Test

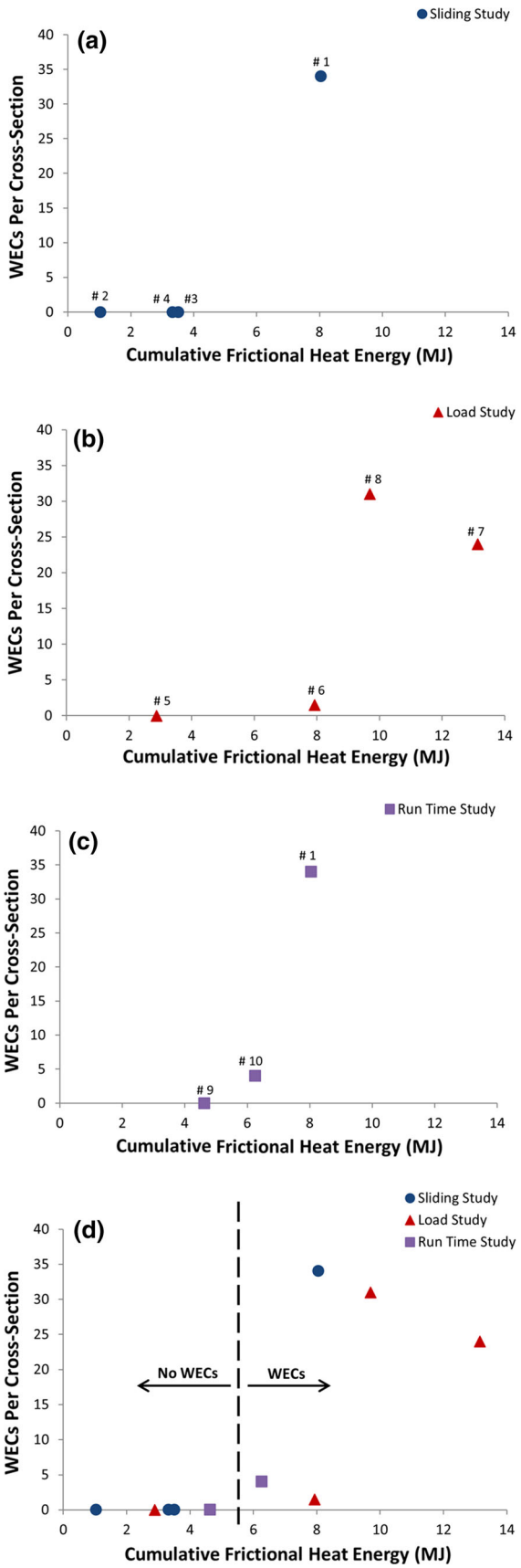

◀**Fig. 5** Cumulative frictional heat energy applied to rollers vs the measure of WECs per cross section for **a** the sliding study, **b** the load study, **c** the run-time study, and **d** all of Tests 1–10. The # in charts **a**–**c** denotes the test number

7 had a larger amount of time to accrue cumulative energy when compared to the tests ran at higher load.

The authors hypothesize that all of the WECs that were generated in this paper initiated at around the same cumulative frictional heat energy regardless of the testing conditions studied (sliding, load, and duration), and also that normal drivers of crack propagation, such as load, determined how long it took for these crack to propagate to failures. Test 12 was designed to prove this theory; Test 12 is an exact repeat of the contact conditions in Test 7; however, instead of allowing this test to reach the run out limit of 100 million cycles, Test 12 was stopped early so that the cumulative frictional heat energy was much closer to the proposed WEC initiation point. A comparison of Test 7 and Test 12 is shown in Fig. 6. This chart shows that the observed number of WECs per cross section did not decrease between these two tests. This finding suggests that the WECs that were observed in Test 7 initiated at around the same cumulative energy as all other tests. This finding confirmed the hypothesis that WEC initiation is based on reaching a cumulative energy threshold, while normal crack propagation drivers, such as normal load, determine the time from WEC initiation to a catastrophic macro-pitting failure.

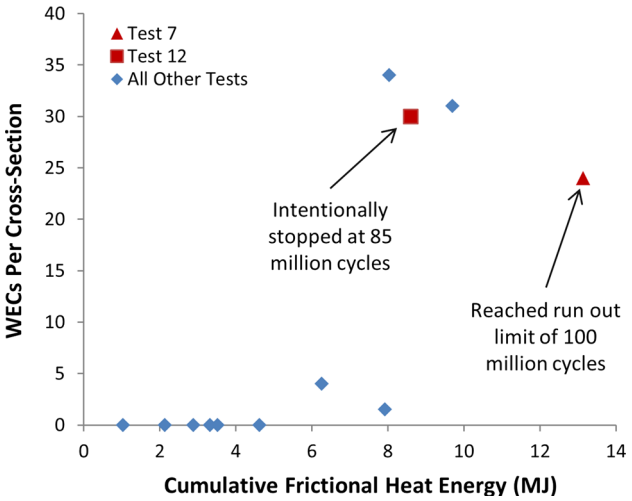

Fig. 6 Cumulative frictional heat energy versus the measure of WECs per cross section with Tests 7 and 12 denoted, Test 7 an exact repeat of the contact conditions in Test 12; however, Test 7 was intentionally stopped early in order to examine the initiation process of WECs

4.2 Dependence of WECs on Rate of Energy Application

It should also be considered that the formation of WECs could be dependent on not only the cumulative energy applied, but also the rate at which energy is applied. If Tests 1 and 8 are compared, some general claims as to the validity of this hypothesis can be made. The contact conditions of these two tests are similar; however, the rolling speed of Test 8 was 3.4 m/s (103 rotations per second), and the rolling speed of Test 1 was 1 m/s (27.2 rotations per second); therefore, Test 8 had ~3.4 times the rate of energy application. These two tests are specially denoted in Fig. 7, and this figure shows that Test 8 had a slightly higher cumulative frictional heat energy. It is postulated that this is due to the fact that the higher rolling speed of Test 8 would also cause a larger film thickness, as well as a higher heat loss to the surrounding oil. Consequently, the authors postulate that, over the energy application rates studies, there is no dependence of WEC initiation on rate of energy application, and that if heat loss to the surrounding environment were taken into account, the cumulative frictional heat energy of Tests 1 and 8 would be almost identical.

4.3 Suppression of Failure Mechanisms Other Than WECs

Since the formation of WECs can be correlated to cumulative frictional heat energy input into a sample, and therefore total test run-time, the suppression of other failure modes that would lead to an early automatic shutdown is critical if WECs are to form. Tests 2, 4, and 11 can be used to illustrate this point; these tests are specifically denoted in Fig. 8. Tests 2 and 4 failed due to surface-initiated macro-pitting; it was previously speculated that this was due to the hydraulic pressurization of oil within surface cracks caused by the positive SRR conditions [10]. Test 11 was designed to have an identical rate of frictional heat energy input as Test 1, and the SRR was halved and the rolling speed was doubled; therefore, the sliding speed is identical between the two tests. It was expected that Test 11 would form WECs after the same amount of time as Test 1 (due to its identical rate of frictional heat energy application). However, it was found that Test 11 failed significantly earlier than Test 1 due to the formation of a large amount of micro-pitting, and a comparison of the surfaces of the roller from Test 1 and Test 11 is shown in Fig. 9. Because of their respective early failures due to mechanisms other than WECs, Tests 2, 4, and 11 terminated before they reached the cumulative energy required to form WECs.

4.4 Interpretation of the Energy Criterion

It should be recognized that the magnitude of the energy threshold is likely to be specific to the testing configuration and conditions presented here. Testing in other lubricants or in other test rigs will likely cause variance in this measure. Also, it should be kept in mind that all of the tests discussed in this paper were performed in a lubricant that is often used to study WEC generation, and that a correlation between WEC generation and cumulative applied frictional heat energy does not imply that the cause of WECs in frictional heat energy. As stated above, the formation of

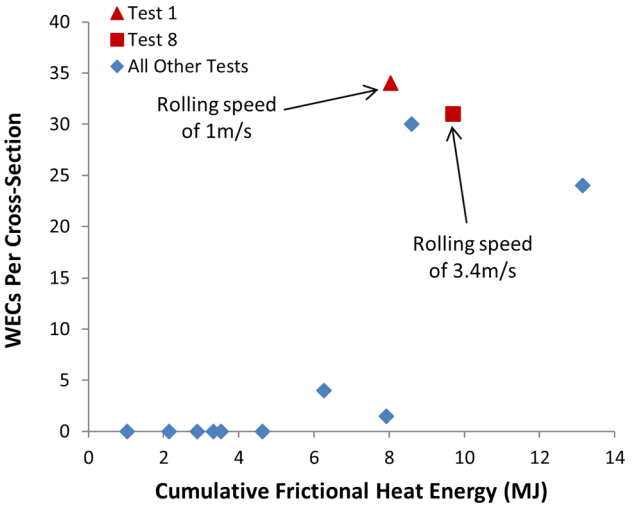

Fig. 7 Cumulative frictional heat energy vs the measure of WECs per cross section with Tests 1 and 8 denoted, and these tests were ran under the same contact conditions; however, the rolling speed of Test 8 was 3.4× that of Test 1, and these tests can be compared to study the influence of the rate of energy application on WEC generation

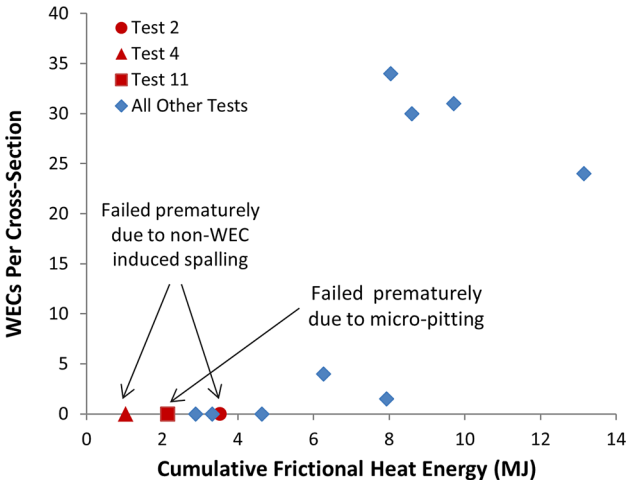

Fig. 8 Cumulative frictional heat energy versus the measure of WECs per cross section with Tests 2, 4, and 11 denoted. These three tests failed due to mechanisms other than WECs, Tests 2 and 4 failed due to non-WEC-induced macro-pitting, and Test 11 failed due to micro-pitting

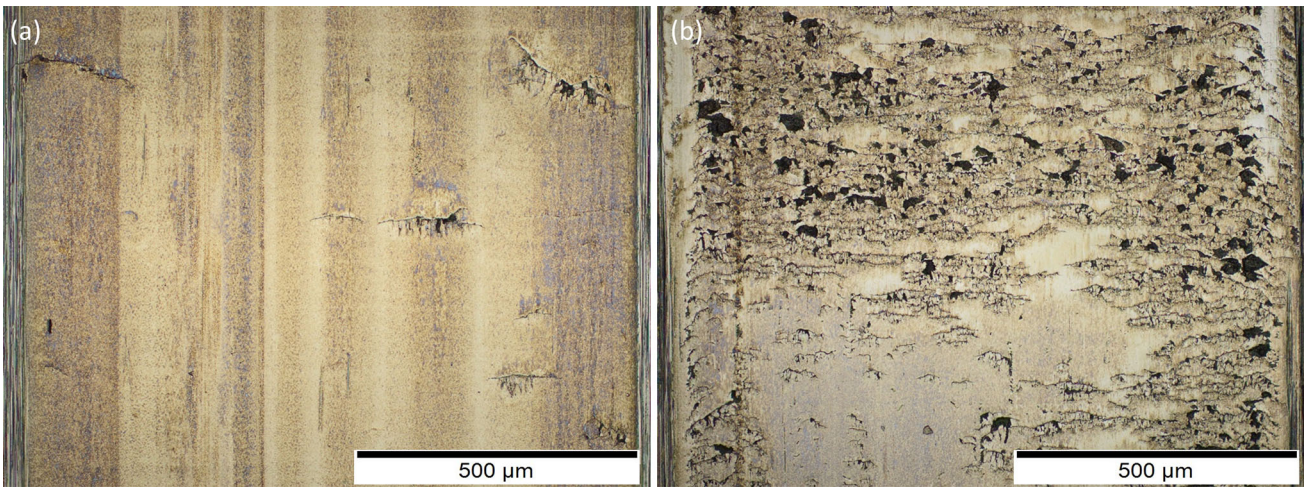

Fig. 9 A comparison of the wear tracks of the test rollers at the conclusion of **a** Test 1 and **b** Test 11. These tests had the same sliding velocity but different SRRs and rolling velocity. Test 1 generated WECs; however, Test 11 failed due to micro-pitting

microstructural alterations or WEAs could be due to any energy source. It is possible that all of the parameters studied here (sliding speed, normal load, and test duration) could aid in WEC generation due to sources other than frictional heat.

4.5 Stages of Microstructural Alterations

The ability to accurately predict the formation of WECs provides a unique opportunity to study the process by which these cracks initiate in bearing steel. Test 10 corresponds to the test that was closest to the proposed initiation point based on the cumulative frictional heat energy criteria. Therefore, in theory, this test should contain WECs that are in their most infantile stage of formation. Throughout the examination of the roller from Test 10, various distinct regions of microstructural alteration and cracking were observed. We interpret these regions to represent discrete stages throughout the sequence of WEC initiation. The first stage consisted of localized dark etching areas (DEAs) without the presence of a crack; examples of this are shown in Fig. 10. We presume that the formation of these DEAs is a precursor to the formation of WECs, which agrees with the findings of others [10–12]. The second observed stage consisted of small, subsurface cracks which are associated with local DEAs, without the presence of WEAs; examples of these cracks are shown in Fig. 11. The third observed stage consists of a crack that has local areas of both dark and white etching; an example of this is shown in Fig. 12. The final observed stage was a fully developed WEC with a large amount of microstructural alteration, as shown in Fig. 13. It should be noted that these four stages were observed in separate locations under the wear track of the roller and therefore were not part of the same crack network.

4.6 Proposed Method of WEC Initiation

Based on the previously discussed optical and SEM observations, as well as the finding that the presence of WECs can be correlated with the cumulative energy applied to a sample, the authors will propose a multistage initiation of WECs based on carbon migration due to high local energy and shear stress. The crystalline structure of tempered martensite (the starting microstructure for the samples used in this study) is body-centered tetrahedral (BCT), and it takes this form due to the fact that a maximum of four carbon atoms become trapped in the lattice during quenching, as illustrated in Fig. 14a. The presence of these carbon atoms in the lattice causes the distortion of the structure to a highly stressed BCT, as opposed to the body-centered cubic (BCC) lattice of ferrite. Within the BCT lattice, lattice lengths A and B are equal and less then C. It is proposed that local inhomogeneities in the steel (carbides, inclusions, voids, etc.) act as concentration points for strain energy, resulting in plasticity, an increase in the dislocation density, and subsequent localized heating. This localized heating, in combination with the applied frictional heat from the contact, causes carbon atoms to progressively diffuse out of the martensite lattice, where they are accommodated at grain boundaries. As these atoms diffuse from local heat-affected lattices, length C, and therefore, the distortion of the BCT lattice decreases [41]. If this process affects multiple lattices in a local area, then this could lead to strain relaxation as a result of the carbon diffusion. If this strain relaxation affects a large

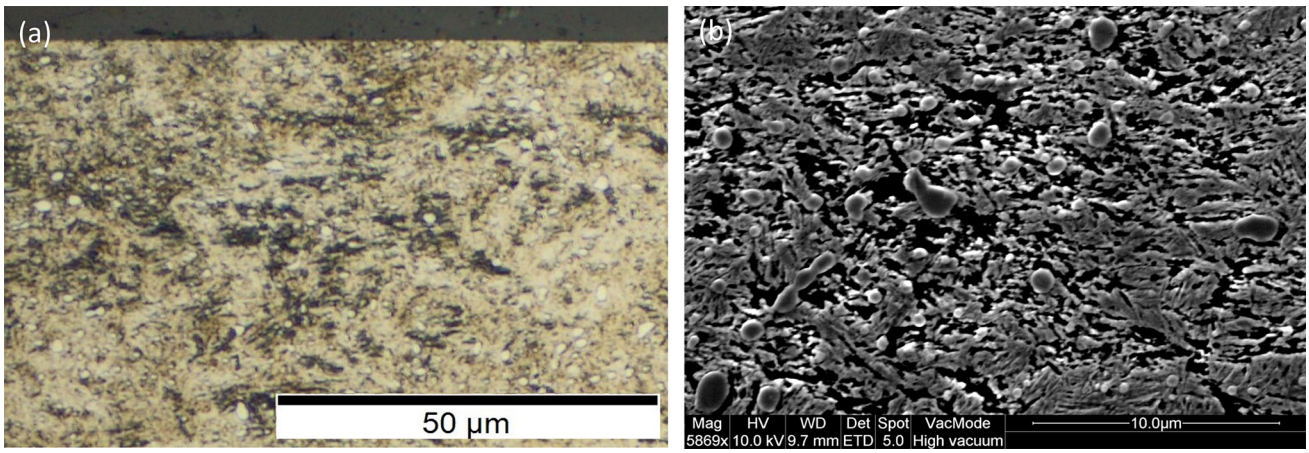

Fig. 10 **a** An optical microscope image and **b** an SEM micrograph showing the DEA without the presence of a crack (stage 1) observed in Test 10

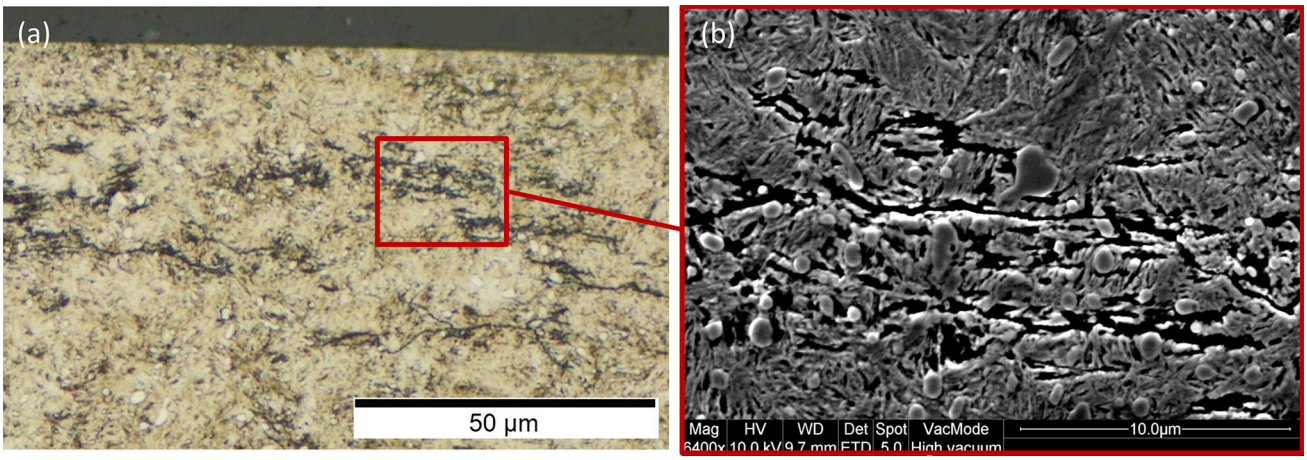

Fig. 11 **a** An optical microscope image and **b** an SEM micrograph showing cracks through regions of DEA without adjacent WEA (stage 2) observed in Test 10

enough area, then an optically observable region containing a carbon-depleted BCT structure surrounded by a carbon-rich boundary would form. If this region was etched, the etchant would pool at the boundary between these structures and the surrounding unrelaxed martensitic matrix and would cause this region to appear as local DEA, such as those that were observed in Fig. 10. Considering that the source of the energy driving this transformation is thought to be both friction heat at the contact and heating due to deformation localized near inhomogeneities, the location of this region relative to the contact surface would likely be at a point where these two sources of energy converge to be at a maximum. Therefore, we would expect these alterations to be localized between the contact surface (where friction heat is maximum) and the depth of maximum shear stress (where the heat due to deformation is maximum).

This process of carbon diffusion and relaxation has some parallels with, and can be thought of similarly to, local non-isothermal tempering. Traditional non-isothermal tempering occurs when a sample is rapidly heated to a tempering temperature and then subsequently cooled, without holding at the aforementioned tempering temperature [42]. Non-isothermal tempering is normally associated with manufacturing processes such as welding; however, it is conceivable that a process similar to this could occur when the surface of a steel roller enters and leaves a high-energy contact such as the ones presented here. The process of non-isothermal tempering is known to lead to high dislocation densities as well as cause the precipitation of carbides [42], similarly to that which has previously been observed in WEC formation [11, 43].

One could imagine that, as energy is continually applied to a region that has been locally altered, and more and more dislocations form, these dislocations could culminate to form a crack through this region of DEA, such as the cracks shown in Fig. 11. The presence of this crack in the steel

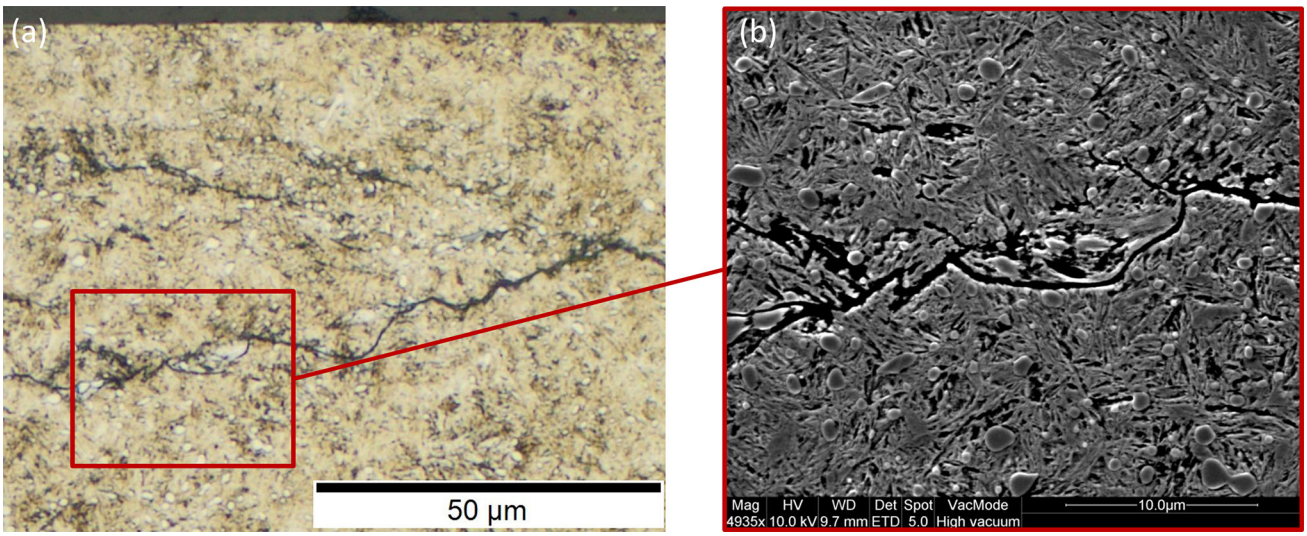

Fig. 12 **a** An optical microscope image and **b** an SEM micrograph showing a crack with a small amount of WEA, DEA, and local carbide deformation (stage 3) observed in Test 10

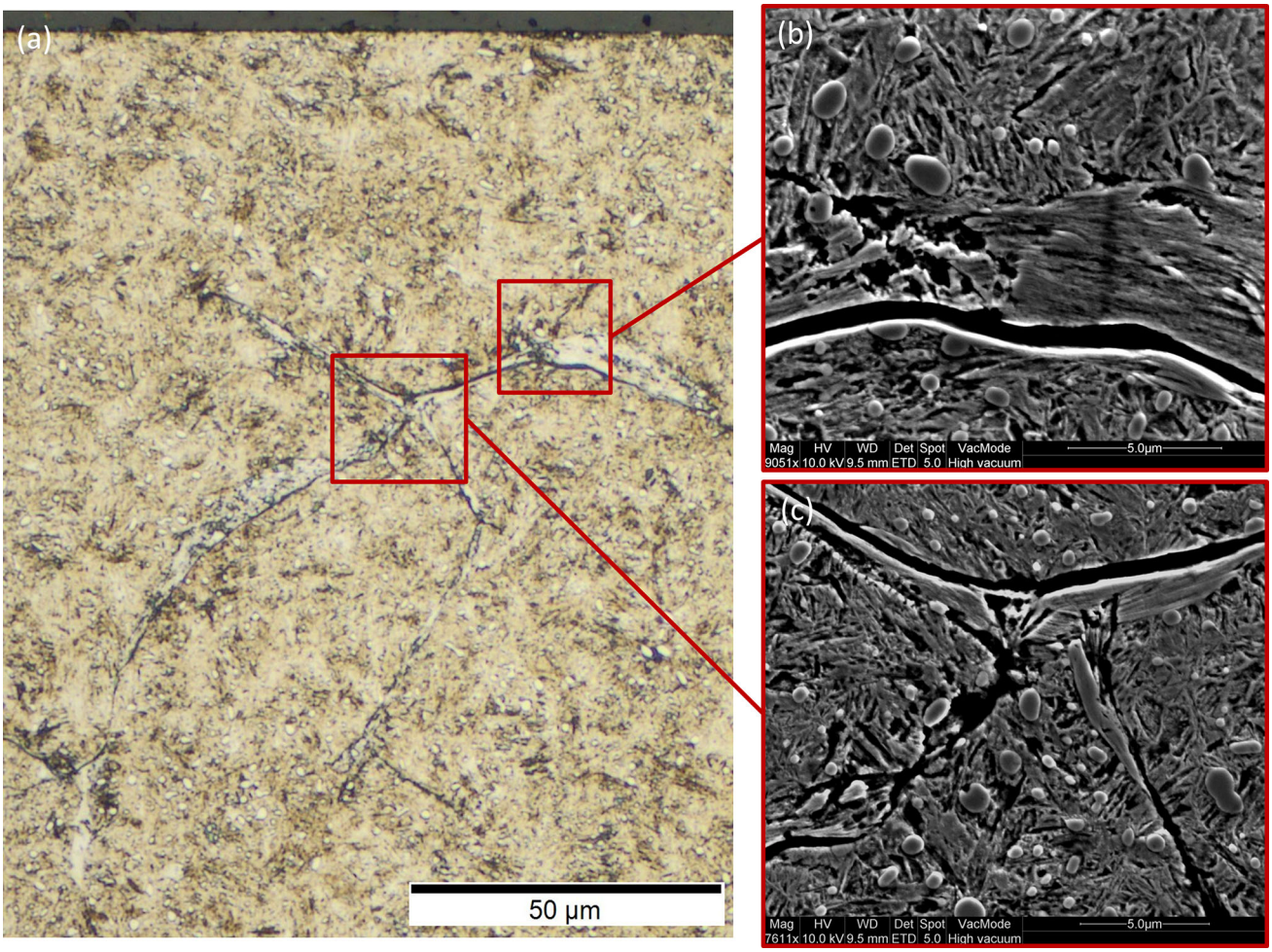

Fig. 13 **a** An optical microscope image and **b** and **c** two SEM micrographs showing a WEC (stage 4) observed in Test 10

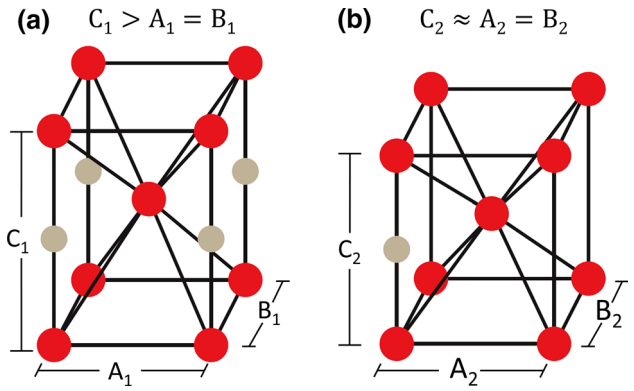

Fig. 14 An illustration showing the BCT lattice of martensite **a** when there are four atoms of carbon trapped within the lattice and **b** when there is only one carbon atom trapped within the lattice. The *red dots* represent iron, and the *gray dots* represent carbon (Color figure online)

would cause significant energy concentration in the areas adjacent to it, which in turn would aid in the formation of additional dislocations. As the density of dislocation increases, they will rearrange in order to form the lowest energy state possible. This will cause grain refinement due to the formation of new cells surrounded by dislocations. This suggests that grain refinement is a gradual process and explains the mixed regions of DEA and WEA that have previously been observed [10]. As carbon continues to diffuse from the BCT lattice, the distortion of the lattice decreases, and therefore, the side length C becomes closer and closer to the lengths of sides A and B, as illustrated in Fig. 14b. It is conceivable that if enough energy is applied to these local regions around the crack, then enough of the carbon atoms that constitute the BCT lattice of martensite could be removed leaving a structure that would appear to be nano-grained supersaturated ferrite surrounded by carbon at its grain boundaries, such as that previously observed in [9]. In this context, the term supersaturated refers to a meta-stable microstructure which contains a higher level of carbon than that of the stable concentration of 0.02 %

This proposed method for WEC initiation is based strictly from optical and SEM observations. Further analysis is needed in order to verify this theory. Work should be done in order to determine the crystalline structure of each of the four distinct stages of WEC initiation discussed above. If this proposed method of WEC initiation is correct, then we would expect to see differences in the distortion of the lattice length C depending upon what stage of WEC initiation is investigated.

The manifestation of WECs has long been a topic of debate. As discussed earlier, it is currently unknown whether the formation of WEA precedes cracks, or whether crack must precede the WEA. The observations shown above provide evidence that the crack precedes the WEA; however, under the current testing conditions, it would seem that the formation of initial microstructural alterations characterized as DEA is a prerequisite to the formation of the crack. Therefore, if the previously proposed method is valid, the same driver, i.e., energy, leads to the formation of the DEA, the crack, and the WEA in that order.

5 Conclusions

The work presented here is, to the author's knowledge, the first attempt to correlate the formation of WECs to the cumulative energy that a sample has experienced. The final conclusions that can be drawn from the current test configuration and results are as follows:

1. A benchtop testing methodology has been developed that can accurately predict the onset of WEC initiation.
2. A correlation was found between the presence of WECs and the cumulative frictional heat energy a sample experienced.
3. The cumulative frictional heat energy associated with WEC initiation seems to be similar regardless of changes in normal load, sliding speed, or run-time. Normal crack propagation drivers such as contact stress seem to determine the amount of time between the initiation of the WEC and the formation of a macro-pit.
4. WECs in their initiation stage were observed in a test that was intentionally stopped early. Within this sample, four distinct stages of crack development were observed: 1) local DEAs without the presence of a crack, 2) cracking through DEA without the presence of WEA, 3) cracks containing local small amount of mixed WEA and DEA, and 4) fully developed WECs. These observations prompted the authors to propose a hypothesis of WEC initiation based on progressive carbon migration out of the martensitic lattice aided by high local energies.
5. Under the conditions presented here, it would appear as though DEA precedes the formation of a crack, and that a crack is required to form the WEA associated with WECs.

Acknowledgments This work is supported by the US Department of Energy Office of Energy Efficiency and Renewable Energy, Wind and Water Power Technology Office under Contract No. DE-AC02-06CH11357. The authors are grateful to DOE Project Managers Mr. Michael Derby and Mr. Nick Johnson for their support and encouragement. The authors would also like to acknowledge the assistance provided by our colleagues at Argonne National Laboratory's Tribology Section, especially Dr. Maria De La Cinta Lorenzo Martin for her assistance with electron microscopy and Dr. Oyelayo Ajayi for his helpful discussion on metallurgy. As well as Dr. David L. Burris of

the University of Delaware's department of Mechanical Engineering for serving as an advisor over the course of this work. The authors would also like to thank Dr. Mihails Scepanskis for many useful conversations pertaining to WEC generation and PCS Instruments for providing samples for the MPR testing. Use of the Center for Nanoscale Materials an Office of Science user facility was supported by the US Department of Energy Office of Science, Office of Basic Energy Sciences under Contract No. DE-AC02-06CH11357.

References

1. Kotzalas, M.N., Doll, G.L.: Tribological advancements for reliable wind turbine performance. Philos. Trans. R. Soc. Lond. Math. Phys. Eng. Sci. **368**, 4829–4850 (2010)
2. Musial, W., Butterfield, S., McNiff, B.: Improving wind turbine gearbox reliability. In: European Wind Energy Conference, Milan, Italy. pp. 7–10 (2007)
3. Spinato, F., Tavner, P.J., Van Bussel, G.J.W., Koutoulakos, E.: Reliability of wind turbine subassemblies. IET Renew. Power Gener. **3**, 387–401 (2009)
4. Sheng, S.: Gearbox Reliability Database: Yesterday, Today, and Tomorrow (Presentation). National Renewable Energy Laboratory (NREL), Golden, CO (2014)
5. Grabulov, A., Petrov, R., Zandbergen, H.W.: EBSD investigation of the crack initiation and TEM/FIB analyses of the microstructural changes around the cracks formed under Rolling Contact Fatigue (RCF). Int. J. Fatigue **32**, 576–583 (2010)
6. Harada, H., Mikami, T., Shibata, M., Sokai, D., Yamamoto, A., Tsubakino, H.: Microstructural changes and crack initiation with white etching area formation under rolling/sliding contact in bearing steel. ISIJ Int. **45**, 1897–1902 (2005)
7. Greco, A., Sheng, S., Keller, J., Erdemir, A.: Material wear and fatigue in wind turbine systems. Wear **302**, 1583–1591 (2013)
8. Loos, J., Bergmann, I., Goss, M.: Influence of currents from electrostatic charges on WEC formation in rolling bearings. Tribol. Trans. (2015). doi:10.1080/10402004.2015.1118582
9. Kang, J.-H., Hosseinkhani, B., Williams, C.A., Moody, M.P., Bagot, P.A.J., Rivera-Díaz-del-Castillo, P.E.J.: Solute redistribution in the nanocrystalline structure formed in bearing steels. Scr. Mater. **69**, 630–633 (2013)
10. Gould, B., Greco, A.: The influence of sliding and contact severity on the generation of white etching cracks. Tribol. Lett. **60**, 1–13 (2015)
11. Becker, P.C.: Microstructural changes around non-metallic inclusions caused by rolling-contact fatigue of ball-bearing steels. Met. Technol. **8**, 234–243 (1981)
12. Gegner, J.: Tribological Aspects of Rolling Bearing Failures. INTECH Open Access Publisher (2011)
13. Uyama, H., Yamada, H., Hidaka, H., Mitamura, N.: The effects of hydrogen on microstructural change and surface originated flaking in rolling contact fatigue. Tribol. Online **6**, 123–132 (2011)
14. Swahn, H., Becker, P.C., Vingsbo, O.: Martensite decay during rolling contact fatigue in ball bearings. Metall. Trans. A **7**, 1099–1110 (1976)
15. Österlund, R., Vingsbo, O.: Phase changes in fatigued ball bearings. Metall. Trans. A **11**, 701–707 (1980)
16. Mitamura, N., Hidaka, H., Takaki, S.: Microstructural development in bearing steel during rolling contact fatigue. In: Materials science forum. pp. 4255–4260. Trans Tech Publications (2007)
17. Hershberger, J., Ajayi, O.O., Zhang, J., Yoon, H., Fenske, G.R.: Evidence of scuffing initiation by adiabatic shear instability. Wear **258**, 1471–1478 (2005)
18. Torrance, A.A., Cameron, A.: Surface transformations in scuffing. Wear **28**, 299–311 (1974)
19. Oila, A., Bull, S.J.: Phase transformations associated with micropitting in rolling/sliding contacts. J. Mater. Sci. **40**, 4767–4774 (2005)
20. Robinski, J., Smurthwaite, D.: Troubleshooting wind gearbox problems. Gear Solut. **8**, 22–33 (2010)
21. Kang, Y.S., Evans, R.D., Doll, G.L.: Roller-raceway slip simulations of wind turbine gearbox bearings using dynamic bearing model. In: STLE/ASME 2010 International Joint Tribology Conference. pp. 407–409. American Society of Mechanical Engineers (2010)
22. Grabulov, A., Ziese, U., Zandbergen, H.W.: TEM/SEM investigation of microstructural changes within the white etching area under rolling contact fatigue and 3-D crack reconstruction by focused ion beam. Scr. Mater. **57**, 635–638 (2007)
23. Ciruna, J.A., Szieleit, H.J.: The effect of hydrogen on the rolling contact fatigue life of AISI 52100 and 440C steel balls. Wear **24**, 107–118 (1973)
24. Grunberg, L.: The formation of hydrogen peroxide on fresh metal surfaces. Proc. Phys. Soc. Sect. B **66**, 153 (1953)
25. Imran, T., Jacobson, B., Shariff, A.: Quantifying diffused hydrogen in AISI-52100 bearing steel and in silver steel under tribo-mechanical action: pure rotating bending, sliding–rotating bending, rolling–rotating bending and uni-axial tensile loading. Wear **261**, 86–95 (2006)
26. Iso, K., Yokouchi, A., Takemura, H.: Research work for clarifying the mechanism of white structure flaking and extending the life of bearings. SAE Technical Paper (2005)
27. Vegter, R.H., Slycke, J.T.: The role of hydrogen on rolling contact fatigue response of rolling element bearings. J. ASTM Int. **7**, 1–12 (2009)
28. Hiraoka, K., Fujimatsu, T., Tsunekage, N., Yamamoto, A.: Generation process observation of micro-structural change in rolling contact fatigue by hydrogen-charged specimens. J. Jpn. Soc. Tribol. **52**, 888–895 (2007)
29. Kino, N., Otani, K.: The influence of hydrogen on rolling contact fatigue life and its improvement. JSAE Rev. **24**, 289–294 (2003)
30. Tamada, K., Tanaka, H.: Occurrence of brittle flaking on bearings used for automotive electrical instruments and auxiliary devices. Wear **199**, 245–252 (1996)
31. Ray, D., Vincent, L., Coquillet, B., Guirandenq, P., Chene, J., Aucouturier, M.: Hydrogen embrittlement of a stainless ball bearing steel. Wear **65**, 103–111 (1980)
32. Matsubara, Y., Hamada, H.: A novel method to evaluate the influence of hydrogen on fatigue properties of high strength steels. J. ASTM Int. **3**, 1–14 (2006)
33. Lü, H., Li, M., Zhang, T., Chu, W.: Hydrogen-enhanced dislocation emission, motion and nucleation of hydrogen-induced cracking for steel. Sci. China Ser. E: Technol. Sci. **40**, 530–538 (1997)
34. Fujita, S., Matsuoka, S., Murakami, Y., Marquis, G.: Effect of hydrogen on mode II fatigue crack behavior of tempered bearing steel and microstructural changes. Int. J. Fatigue **32**, 943–951 (2010)
35. Evans, M.-H., Richardson, A.D., Wang, L., Wood, R.J.K.: Effect of hydrogen on butterfly and white etching crack (WEC) formation under rolling contact fatigue (RCF). Wear **306**, 226–241 (2013)
36. Ruellan, A., Ville, F., Kleber, X., Arnaudon, A., Girodin, D.: Understanding white etching cracks in rolling element bearings: the effect of hydrogen charging on the formation mechanisms. Proc. Inst. Mech. Eng. Part J J. Eng. Tribol. **228**, 1252–1265 (2014)
37. Evans, M.-H., Wang, L., Jones, H., Wood, R.J.K.: White etching crack (WEC) investigation by serial sectioning, focused ion beam and 3-D crack modelling. Tribol. Int. **65**, 146–160 (2013)

38. Holweger, W., Wolf, M., Merk, D., Blass, T., Goss, M., Loos, J., Barteldes, S., Jakovics, A.: White etching crack root cause investigations. Tribol. Trans. **58**, 59–69 (2015)
39. Evans, M.-H., Richardson, A.D., Wang, L., Wood, R.J.K., Anderson, W.B.: Confirming subsurface initiation at non-metallic inclusions as one mechanism for white etching crack (WEC) formation. Tribol. Int. **75**, 87–97 (2014)
40. Evans, M.-H., Richardson, A.D., Wang, L., Wood, R.J.K.: Serial sectioning investigation of butterfly and white etching crack (WEC) formation in wind turbine gearbox bearings. Wear **302**, 1573–1582 (2013)
41. Leslie, W.: The Physical Metallurgy of Steels. Hemisphere Publishing Corporation, Mcgraw-Hill Book Company, Washington, New York, London (1981)
42. Hernandez, V.B., Nayak, S.S., Zhou, Y.: Tempering of martensite in dual-phase steels and its effects on softening behavior. Metall. Mater. Trans. A **42**, 3115–3129 (2011)
43. Evans, M.-H., Walker, J.C., Ma, C., Wang, L., Wood, R.J.K.: A FIB/TEM study of butterfly crack formation and white etching area (WEA) microstructural changes under rolling contact fatigue in 100Cr6 bearing steel. Mater. Sci. Eng. A **570**, 127–134 (2013)